Comparative study of ZnO and ZnFe2O4 micro and nanoparticle-based screen-printed electrodes in pH sensing

Original
Comparative study of ZnO and ZnFe2O4 micro and nanoparticle-based screen-printed electrodes in pH sensing / Madagalam, M., Franceschini, F., Fernandes, C., Rosito, M., Padovano, E., Carrara, S., Tagliaferro, A., Bartoli, M., Taurino, I.. - In: IEEE SENSORS JOURNAL. - ISSN 1530-437X. - ELETTRONICO. - 25:7(2025), pp. 10602-10612. [10.1109/jsen.2025.3543243]

Publisher:
IEEE

Published
DOI:10.1109/jsen.2025.3543243

AUTHOR QUERIES

AUTHOR PLEASE ANSWER ALL QUERIES

PLEASE NOTE: We cannot accept new source files as corrections for your article. If possible, please annotate the PDF proof we have sent you with your corrections and upload it via the Author Gateway. Alternatively, you may send us your corrections in list format. You may also upload revised graphics via the Author Gateway.

Carefully check the page proofs (and coordinate with all authors); additional changes or updates WILL NOT be accepted after the article is published online/print in its final form. Please check author names and affiliations, funding, as well as the overall article for any errors prior to sending in your author proof corrections.

AQ:1 = Please note that “Micro and Nanoparticle-based” has been changed as “Microparticle and Nanoparticle-Based” in the article title. Please check and confirm.

AQ:2 = Please confirm or add details for any funding or financial support for the research of this article.

AQ:3 = Please confirm the expansion for the acronym XRD.

AQ:4 = Please confirm whether the edits made in the current affiliation of all the authors are correct.

AQ:5 = Please confirm the city name for Politecnico di Torino.

AQ:6 = Please confirm whether the edits made in the sentence “Mallikarjun Madagalam. . .electrochemical interfaces” are correct.

AQ:7 = Please provide the year of completion when the author Filippo Franceschini received the B.Sc. and M.Sc. degrees.

AQ:8 = Please confirm the retention of the sentence “as an FWO Fellow (Strategic Basic Research).” is correct.

AQ:9 = Please provide the year of completion when the author Sandro Carrara received the Ph.D., master’s, and Diploma degrees.

AQ:10 = The term “Chairman” is considered non-inclusive. Please identify a replacement term from the Inclusive Language Guide found in the IEEE Editorial Style Manual: https://journals.ieeeauthorcenter.ieee.org/wp-content/uploads/sites/7/IEEE-Editorial-Style-Manual-for-Authors.pdf

AQ:11 = Please provide a better/higher quality image for the author “Alberto Tagliaferro.”

AQ:12 = Please provide the year of completion when the author Alberto Tagliaferro received the M.Sc. and Ph.D. degrees.

AQ:13 = Please provide the location (city, state code, country) for University of Alberta.

AQ:14 = Please provide the year of completion when the author Irene Taurino received the B.Sc. and dual M.Sc. degrees.

AQ:15 = Please provide the location (city, country) for Aerosol Science and Technology.

AQ:1

Comparative Study of ZnO and $ZnFe_2O_4$ Microparticle and Nanoparticle-Based Screen-Printed Electrodes in pH Sensing

Mallikarjun Madagalam, *Student Member, IEEE*, Filippo Franceschini, *Student Member, IEEE*, Catarina Fernandes, Michele Rosito, Elisa Padovano, Sandro Carrara, *Fellow, IEEE*, Alberto Tagliaferro, Mattia Bartoli, and Irene Taurino, *Member, IEEE*

***Abstract*—This work presents the application of zinc oxide (ZnO) and zinc ferrite ($ZnFe_2O_4$) for electrochemical pH sensing. ZnO and $ZnFe_2O_4$ are synthesized by auto-combustion synthesis method. Field emission scanning electron microroscopic (FESEM) images revealed that ZnO particles have pyramid- and spherical-shaped morphology with micrometer dimensions, while $ZnFe_2O_4$ particles have spherical shape at the nanoscale. The surface-modified screen-printed electrodes with ZnO and $ZnFe_2O_4$ particles are initially characterized by the ferri/ferrocyanide redox couple. Significant improvement in sensitivity (bare carbon: 6.3 ± 0.4 μA/mM, ZnO: 8.5 ± 0.3 μA/mM, $ZnFe_2O_4$: 8.9 ± 0.5 μA/mM) and rate constant (bare carbon: 10 ± 1 ms^{-1}, ZnO: 46 ± 4 ms^{-1}, $ZnFe_2O_4$: 42 ± 3 ms^{-1}) is observed with the surface-modified sensors. Chronopotentiometric pH response of the sensors showed hysteresis behavior with pH loop. No interference effects are observed, and the pH sensitivity of the bare carbon sensor (23.9 ± 1.4 mV/pH) is increased by the introduction of ZnO (38.1 ± 1.3 mV/pH) and $ZnFe_2O_4$ (37.2 ± 1.1 mV/pH) particles. Stability of the pH response is discussed, and ways for its improvement are proposed.**

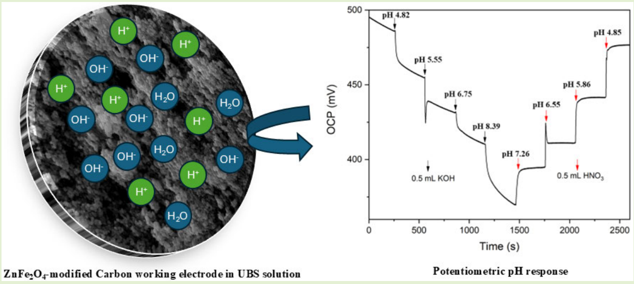

***Index Terms*—Microparticles, nanoparticles, potentiometric pH sensor, sensor stability, zinc ferrite ($ZnFe_2O_4$), zinc oxide (ZnO).**

I. INTRODUCTION

ELECTROCHEMICAL pH sensing is valued for its high sensitivity, rapid response, and adaptability to a wide range of environments, making it a versatile solution in fields such as clinical diagnostics [1], environmental monitoring [2], water quality assessment [3], [4], and industrial process control [5]. These sensors operate based on the electrochemical interaction between a pH-sensitive material and hydrogen ions (H^+) in a solution, allowing for real-time, in situ measurements of acidity, neutrality, or alkalinity of a solution [6].

Electrochemical pH sensors typically work through potentiometric, amperometric, or conductometric approaches. The most common type is the potentiometric pH sensor, which measures the potential difference between a pH-sensitive working electrode (WE) (such as glass electrodes or metal oxides) and a reference electrode (RE) (typically Ag/AgCl) immersed in the solution. The potential generated at the WE is proportional to the activity of H^+ ions, which are related to the solution's pH value through Nernst equation [6], [7], [8].

Metal oxide nanomaterials have emerged as highly effective materials for electrochemical pH sensing due to their excellent electrochemical properties, stability, and sensitivity to hydrogen ions (H^+) in solutions. Their unique structural, electrical, and chemical characteristics make them suitable for a wide range of pH sensing applications [1], [6], [9], [10]. In environmental applications, titanium dioxide (TiO_2) [11] and zinc oxide (ZnO) [3], [12] nanomaterials have been employed in pH sensors to monitor water quality due to their wide bandgap [13], [14]. These sensors can detect shifts in pH caused by contaminants in rivers, lakes, or oceans, providing crucial data for water management. Nickel oxide (NiO) [15] and copper oxide (CuO) [6], [9], [16] nanoparticles are also commonly used in soil pH sensors due to their robust sensing capabilities in harsh environments.

In clinical diagnostics, monitoring pH is vital for tracking physiological parameters such as blood acidity (pH of blood)

AQ:2

Received 3 January 2025; accepted 4 February 2025. The associate editor coordinating the review of this article and approving it for publication was Dr. Xiaoshan Zhu. *(Corresponding author: Mallikarjun Madagalam.)*

Please see the Acknowledgment section of this article for the author affiliations.

This article has supplementary downloadable material available at https://doi.org/10.1109/JSEN.2025.3543243, provided by the authors.

Digital Object Identifier 10.1109/JSEN.2025.3543243

or the pH of interstitial fluids, which are critical in conditions like acidosis or alkalosis [1]. Iridium oxide (IrO_x) [8], [17] and ruthenium oxide (RuO_2) [1], [6], [10], [18], [19] are used to develop pH sensors with super Nernstian behavior that can be integrated into biomedical devices, including wearable and implantable sensors. These materials exhibit fast response times and stability under physiological conditions. Tin oxide (SnO_2) [6], [18], [20] nanomaterials are also explored for implantable pH sensors due to their nontoxic nature and high sensitivity to pH changes, which are essential features for detecting pH changes in tissue environments during medical treatments. Tungsten oxide (WO_3) is also used to develop pH sensors for clinical diagnostics [21], [22].

Spinel oxides are another class of multitransition metal oxides such as zinc ferrite ($ZnFe_2O_4$) and nickel ferrite ($NiFe_2O_4$). The spinels possess a crystal structure of the form AB_2O_4 (A—metal cation with "+2" oxidation state and B—metal cation with "+3" oxidation state) with excellent chemical stability and electrical neutrality [23]. Several spinel oxide nanomaterials are used as sensing materials in electrochemical sensing applications for drug detection [24]. An improvement of the electrochemical sensing response is possible due to the tunability of their crystal structure. Their composition can be easily modified maintaining the chemical stability of the structure [25], [26], [27], [28], [29]. The spinel can be normal, inverse, or mixed with different cations occupying different sites in the crystal structure and leading to different electrochemical performance due to the change in their semiconducting nature either from p to n or from n- to p-type [25], [26]. The magnetic nature (ferromagnetic and antiferromagnetic behavior leading to electron scattering effects and charge trapping) of the spinel materials also plays an important role in the conductivity of spinel oxides [30] which in turn can affect the electrochemical sensing performance. This class of spinel nanomaterials is not explored as pH sensing electrode materials in the literature as far as our knowledge is concerned. Therefore, in this work, we investigate the capability of $ZnFe_2O_4$ normal spinel material to act as an electrode sensing material of pH.

ZnO and $ZnFe_2O_4$ particles are synthesized and characterized using different techniques. Commercial screen-printed electrodes (SPEs) are used as an electrochemical sensing cell and the surface of the WE is modified with the newly synthesized materials. The electrochemical behavior of the new sensors is first assessed using the well-known ferri/ferrocyanide probe molecule, then their performance as pH sensors is assessed. Different performance characteristics of pH sensors such as hysteresis, sensor stability, sensitivity, and interference effects are presented and discussed.

II. MATERIALS AND METHODS

A. Chemicals

Zinc nitrate ($Zn(NO_3)_2{\cdot}6H_2O$), iron nitrate ($Fe(NO_3)_3{\cdot}9H_2O$), $C(NH_2)_2O$ (Urea), Butanol ($C_4H_{10}O$), potassium hexacyanoferrate(II) ($K_4Fe(CN)_6$), potassium hexacyanoferrate(III) ($K_3Fe(CN)_6$), acetic acid (CH_3COOH), potassium nitrate (KNO_3), boric acid (H_3BO_3), phosphoric acid (H_3PO_4), potassium hydroxide (KOH), and nitric acid (HNO_3) are purchased from Sigma Aldrich and used without any further purification.

B. Material Synthesis

A simple and cost-effective auto-combustion synthesis is used to synthesize nanomaterials based on our previous work [25]. Synthesis of $ZnFe_2O_4$ nanoparticles is reported in our previous work [25], [31]. ZnO is synthesized by using only $Zn(NO_3)_2{\cdot}6H_2O$ following the same process as $ZnFe_2O_4$ synthesis.

C. Preparation of Universal Buffer Solution (UBS)

UBS covering the pH range from 2 to 12 is prepared to characterize electrochemical sensors. A measure of 0.3 mL (0.01 M) of CH_3COOH, 5.05 g (0.1 M) of KNO_3, 0.31 g (0.01 M) of H_3BO_3, and 0.58 mL (0.01 M) of H_3PO_4 are mixed with 0.5 L of deionized (DI) water in a glass container. The mixture is kept in an ultrasonic bath for 5 min to dissolve all the chemicals and obtain a final homogeneous solution.

D. Apparatus

Field emission scanning electron microroscopic (FESEM) images are collected utilizing a Zeis SupraTM 50 (Oberkochen, Germany) to examine the nanomaterial's morphology. The crystal structure of the materials is determined by X-ray powder diffraction (XRD) using a Panalytical Empyrean diffractometer (Malvern Panalytical, Malvern, U.K.). The XRD analysis of the powder samples is performed at room temperature using a Bragg–Brentano setup with Cu Kα ($\lambda = 1.5418$ Å) radiation at 40 kV and a current of 40 mA. The analysis is carried out using a time step of 60 s and a step size of 0.013°/s, covering a 2θ range from 10° to 70°. Palmsens potentiostat with PSTrace 5.9 is used to perform cyclic voltammetry (CV) in solutions containing ferri/ferrocyanide. Metrohm Autolab with Nova 2.1 is used for electrochemical impedance spectroscopic (EIS) studies and chronopotentiometric pH sensing.

AQ:3

E. Electrochemical Sensors

Commercial screen-printed carbon WE (area 0.12 cm^2) and carbon counter electrode (CE) on a ceramic substrate along with an external double junction Ag/AgCl RE are used as electrodes for ferri/ferrocyanide sensing. The same method as reported in the literature [25] is adopted to prepare the nanomaterial solutions and the surface of the carbon WE is modified using the drop-casting technique as reported previously [25], [31], [32].

F. Electrochemical Measurements

CV is used to characterize the sensors performance for the detection of ferri/ferrocyanide redox couple with a potential window ranging from −0.4 to 0.8 V at a scan rate of 100 mV/s in phosphate buffer (PB) at pH 7. Scan rate analysis is performed by changing the scan rate from 25 mV/s to 125 mV/s in steps of 25 mV/s. Calibration of the sensors is conducted by recording cyclic voltammograms in the concentration range

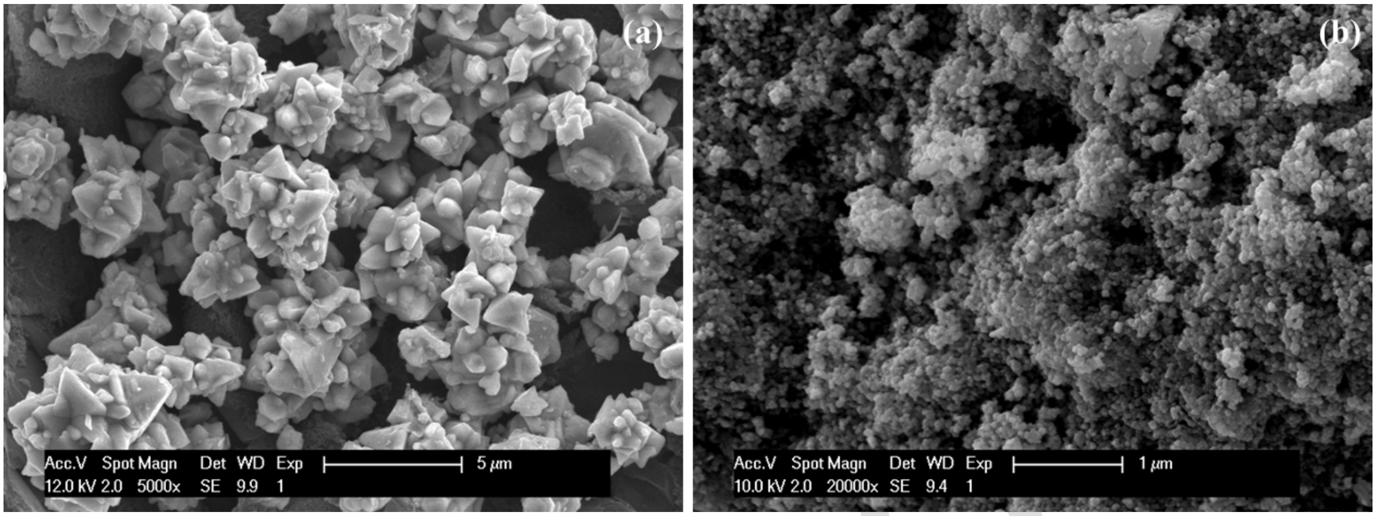

Fig. 1. FESEM images of (a) ZnO with 5k× and (b) $ZnFe_2O_4$ with 20k× magnification, respectively.

from 1 to 8 mM of ferri/ferrocyanide redox couple. EIS is performed in the frequency from 0.1 to 100 kHz with 10 points/decade at an amplitude of 5 mV. Chronopotentiometric experiments are conducted for pH initially in the full loop of 2-12-2 and in the physiologically relevant pH range of 5–8.5. The RE and CE probes of the Autolab are coupled together, and the solution is continuously stirred at 500 r/min. Open-circuit potential (OCP) is recorded with time and the average of the last 60 s of the response of OCP before any pH change in solution is plotted against the pH value for the calibration. The slope of the plot is reported as the sensitivity of the sensors. Interference measurements are conducted using 30 mM KCl and 5 mM NaCl to verify the robustness of the sensor toward interfering ions.

III. RESULTS AND DISCUSSION

A. Material Characterization

Fig. 1 shows the FESEM images of ZnO and $ZnFe_2O_4$ particles-modified carbon surface. ZnO particles have a pyramid shape at microscale, while some smaller particles exhibit a different morphology like spherical one. $ZnFe_2O_4$ particles show spherical-shaped morphology. A certain amount of aggregation is observed in both materials that are possibly due to the adopted synthesis method [25], [33] as it provides a weak control over the particle growth kinetics.

The XRD patterns of $ZnFe_2O_4$ and ZnO are shown in Fig. 2. For $ZnFe_2O_4$, the experimental pattern fully matches with the normal spinel Franklinite ($ZnFe_2O_4$, reference code 01-089-4926). Some low-intensity peaks are noticed in the 2θ range between 30° and 37°: these peaks are compatible with the most intense peaks of ZnO (reference code 01-080-0075) and iron oxide (Fe_2O_3, reference code 01-085-0987) in accordance with previous studies [25], [26]. For ZnO, the XRD pattern neatly matches with the ZnO one (reference code 01-080-0075). The low-intensity peak at low angles is attributed to graphite, which might be present as an impurity due to the graphite reactor used for the material synthesis. Crystallite size of the materials is calculated using Scherrer's method [25], [26]. $ZnFe_2O_4$ has an average crystallite size of 35.2 ± 3.3 nm, while ZnO has an average crystallite size of 45.7 ± 1.3 nm. In the case of ZnO-particles, particles are formed by abnormal asymmetric growth leading to the micrometer dimensions of particles, as evidenced in Fig. 1.

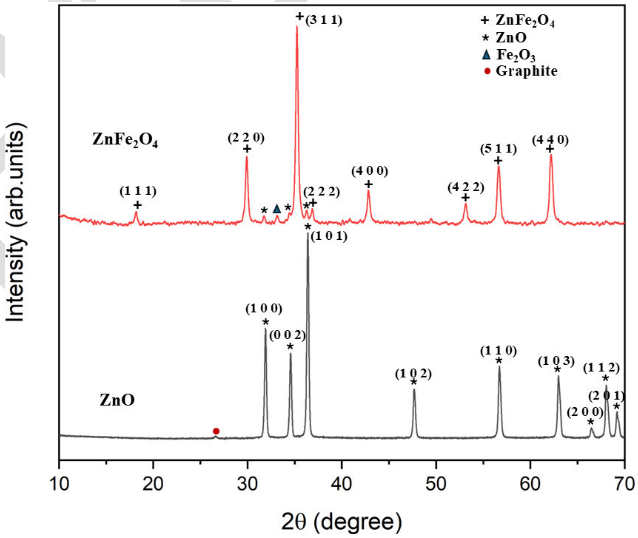

Fig. 2. XRD patterns of $ZnFe_2O_4$ and ZnO particles synthesized by auto-combustion.

B. Electrochemical Characterization

Fig. 3 shows the cyclic voltammograms of the bare, $ZnFe_2O_4$, and ZnO sensors characterized in 4 mM ferri/ferrocyanide redox couple in 0.1 M PB at pH 7 at a scan rate of 100 mV/s. The introduction of nanostructured/microstructured materials has enhanced the performance of screen-printed carbon electrodes. The oxidation peak current (I_{pa}) is increased [~14 μA: $I_{pa} = 44.1 \pm 0.6\ \mu$A ($ZnFe_2O_4$), 44.3 ± 0.4 μA (ZnO)] and the anodic peak potential (oxidation peak potential: E_{pa}) is decreased [~70 mV: $E_{pa} = 413 \pm 3$ ($ZnFe_2O_4$), 407 ± 3 mV (ZnO)] compared to bare carbon sensor ($I_{pa} = 30.6 \pm 1.4\ \mu$A, $E_{pa} = 483 \pm 7$ mV).

Cyclic voltammograms obtained at various scan rates are depicted in Fig. S1 for bare carbon, $ZnFe_2O_4$, and ZnO sensors. The anodic (I_{pa}) and cathodic peak currents (I_{pc})

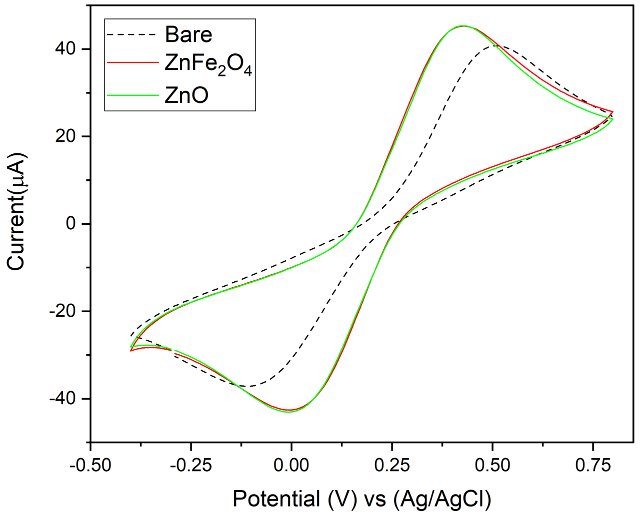

Fig. 3. Cyclic voltammograms of different sensors at a scan rate of 100 mV/s. (Electrolytic solution: 4 mM ferri/ferrocyanide in PB (0.1 M) at pH 7).

TABLE I

ELECTROACTIVE SURFACE AREA AND INTERFACE IMPEDANCES IN CHARACTERIZING FERRI/FERROCYANIDE REDOX COUPLE ON BARE CARBON AND SURFACE-MODIFIED SENSORS

Sensor	A_{RS} (cm^2)	R_s(Ω)	R_p(kΩ)
Bare	0.27 ± 0.05	166	17.2
ZnFe$_2$O$_4$	0.49 ± 0.03	146	13.4
ZnO	0.49 ± 0.02	139	11.8

increased with the increase in scan rate and varied linearly with the square root of the scan rate ($\sqrt{\nu}$) in the range 25–125 mV/s, as shown in Fig. S2. The peak currents linear regression equations with their regression coefficients, confirming the high level of linearity, are listed in Table S1. Absolute redox current peak values are plotted in Fig. S3 to show the differences between the oxidation and reduction peak currents. The redox peak current ratios with scan rate are reported in Table S2, and the ratio $I_{\mathrm{pa}}/I_{\mathrm{pc}}$ is ≈1. Electroactive surface area (A_{RS}) of the sensors is calculated using Randles–Sevčik equation [26] and reported in Table I. It is observed that the electroactive surface area of the sensors is increased due to the presence of nanoparticle/microparticle of ZnFe$_2$O$_4$/ZnO on the carbon surface compared to the bare carbon sensor. Both ZnFe$_2$O$_4$ and ZnO-based sensors have a similar electroactive surface area indicating the same loading of the nanoparticle/microparticle on the carbon surface that participates in the electrochemical reaction with ferri/ferrocyanide redox couple.

The peak-to-peak separation ($\Delta E_p = E_{\mathrm{pa}} - E_{\mathrm{pc}}$, where E_{pc} is the cathodic peak potential or reduction peak potential) lowered by 150 mV compared to bare carbon sensor due to the presence of either ZnO or ZnFe$_2$O$_4$ particles. The ZnO-based sensor showed the lowest ΔE_p of 387 ± 9 mV, while the ZnFe$_2$O$_4$ sensor and bare carbon sensor exhibited a ΔE_p of 397 ± 7 and 547 ± 9 mV, respectively. As the electron transfer kinetics are directly related to ΔE_p, the lower ΔE_p indicates faster electrochemical reactions with high reversibility. In Figs. S4 and S5, the redox peak positions E_{pa} and E_{pc}, and ΔE_p are plotted and a linear variation against $\ln(\nu)$ is observed. The linear regression equations with their coefficients are reported in Tables S3 and S4, respectively. Half-potential ($E_{1/2} = (E_{\mathrm{pa}} + E_{\mathrm{pc}})/2$) is shown in Fig. S6 and has almost a constant relation with $\ln(\nu)$ is observed. The redox peak current ratio, ΔE_p, and $E_{1/2}$ suggest that the interface is a quasi-reversible electrochemical interface from Randles–Sevčik theory [34], [35]. Following the equations from the Laviron model [25], [36], [37], the electron transfer rate coefficient "α" and kinetic rate constant "k," using ΔE_p ($\nu = 100$ mV/s) and $n = 1$, are calculated and presented in Table II.

EIS is performed to study the impedance properties of the electrochemical interface between 4 mM ferri/ferrocyanide redox couple and different sensors. Nyquist plots of bare, ZnFe$_2$O$_4$, and ZnO-based sensors are reported in Fig. 4. The Nyquist profiles of the sensors show only semicircles

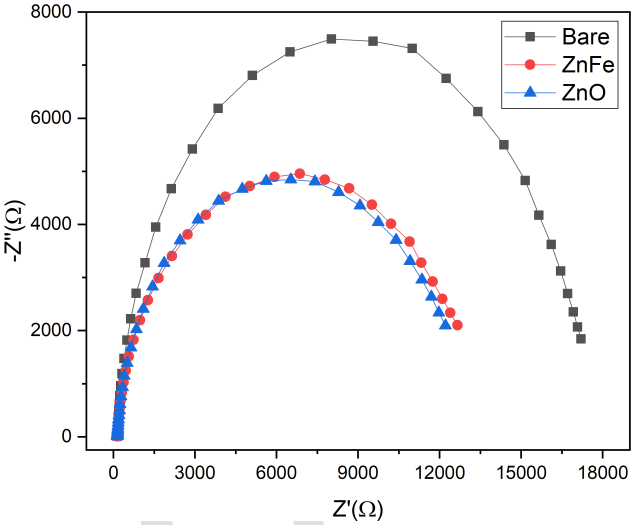

Fig. 4. Nyquist plots of different sensors in 4 mM ferri/ferrocyanide in PB (0.1 M) at pH 7. Frequency range is 0.5–100 kHz with 10 points per decade at an amplitude of 5 mV.

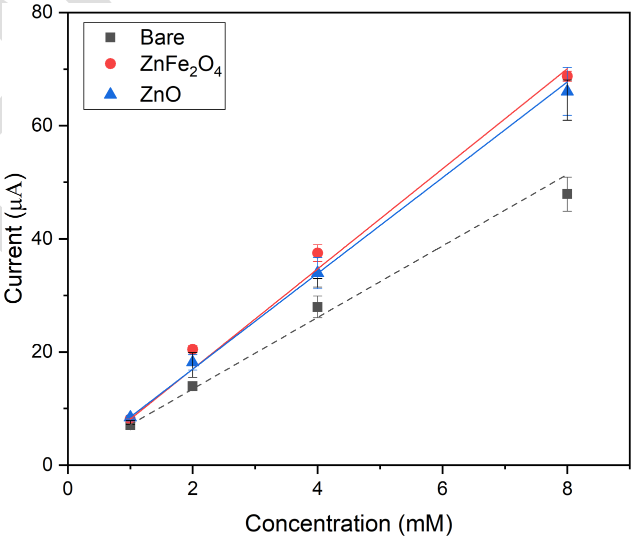

Fig. 5. Calibration of sensors for concentrations of ferri/ferrocyanide redox couple in PB (0.1 M) up to 8 mM.

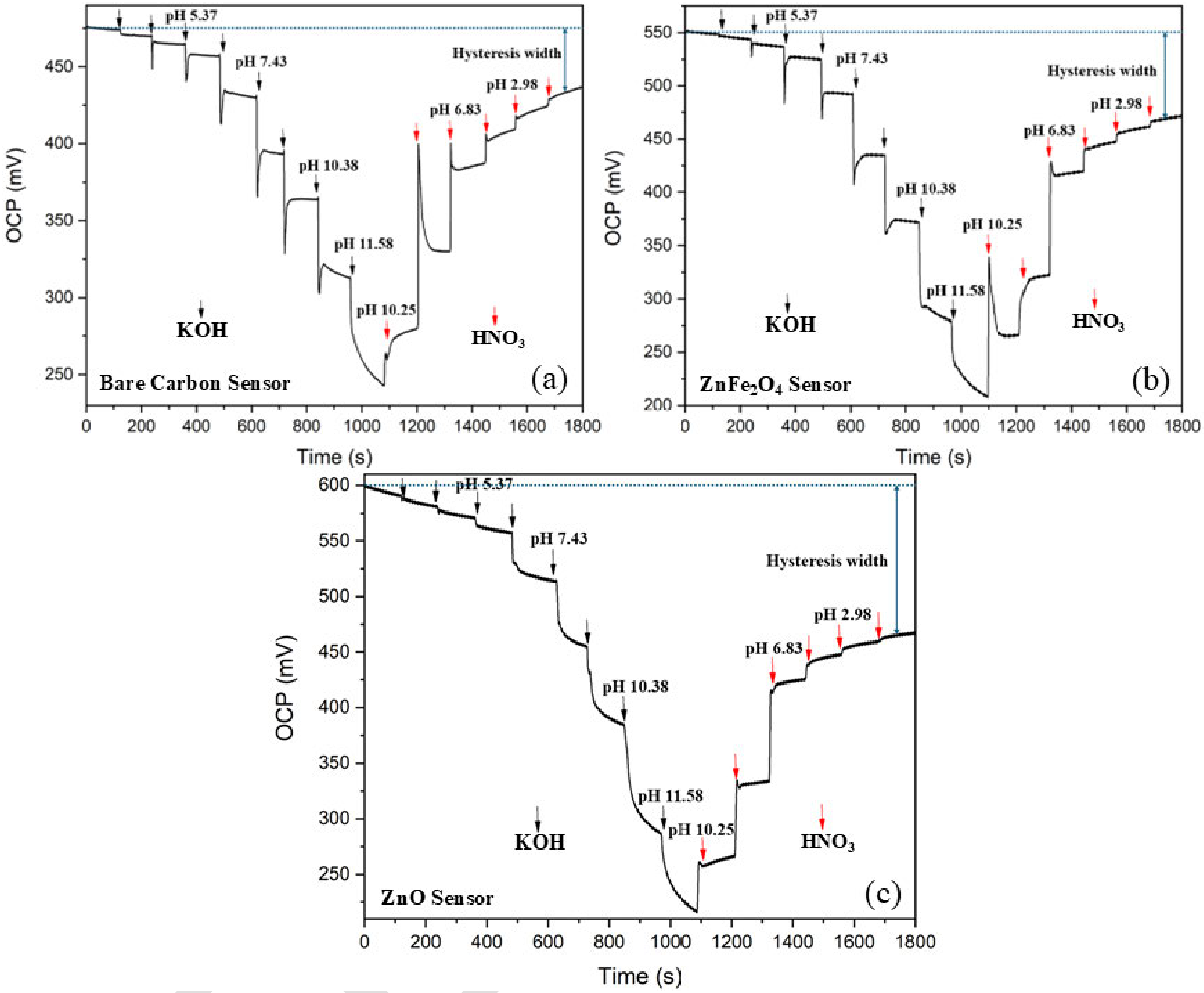

Fig. 6. Chronopotentiometric response of (a) bare, (b) $ZnFe_2O_4$, and (c) ZnO pH sensors showing the hysteresis effect in pH loop 2-12-2.

TABLE II

ELECTROCHEMICAL PARAMETERS IN CHARACTERIZING FERRI/FERROCYANIDE REDOX COUPLE ON BARE CARBON AND SURFACE-MODIFIED SENSORS

Sensor	α	ΔE_P(mV)	k (ms^{-1})
Bare	0.47 ± 0.01	547 ± 9	9.97 ± 0.78
$ZnFe_2O_4$	0.49 ± 0.01	397 ± 7	41.8 ± 2.6
ZnO	0.496 ± 0.002	387 ± 9	46 ± 4

associated with charge transfer kinetic limitations. Therefore, Randles equivalent circuit model with a series resistance (R_s), charge transfer resistance (R_p), and a constant phase element (CPE) are used to fit the obtained Nyquist plots of bare, $ZnFe_2O_4$, and ZnO-modified sensors without any Warburg impedance (diffusion-controlled) as shown in Fig. S7. From the circuit fitting, series (solution) resistance (R_s) and charge transfer resistance (R_p) of the sensors are extracted and reported in Table I. The charge transfer resistance of the $ZnFe_2O_4$ and ZnO-based sensors is significantly lower than the bare carbon sensor supporting the higher electron transfer rate constant. ZnO-based sensor showed 1.6 kΩ lower charge transfer resistance with similar CPE parameters compared to $ZnFe_2O_4$-based sensor supporting its higher electron transfer rate (higher "k").

The sensors are calibrated by taking the average response of three sensors of each type, and the calibration plots are shown in Fig. 5. Sensitivity is computed with reference to the oxidation peaks of the ferri/ferrocyanide redox couple in the concentration range 1–8 mM. The bare carbon sensor has a sensitivity of 6.3 ± 0.4 μA/mM, while the $ZnFe_2O_4$-based sensor and the ZnO-based sensor have sensitivities of 8.9 ± 0.5 and 8.5 ± 0.3 μA/mM, respectively. Though there are significant differences in crystallite size and morphology, the materials have shown similar electrochemical performance (k and sensitivity) which might be due to their similar electroactive surface area and charge transfer resistance.

Fig. 6 shows the chronopotentiometric response of bare carbon, $ZnFe_2O_4$, and ZnO-based sensors in the full pH loop of 2-12-2 (with 15 different pH values reported in the supporting information Table S5). The response at each pH is measured for two minutes (total time span of 30 min), and it is observed that ZnO has the higher initial OCP (lowest pH values). Moreover, there is huge shift in OCP after pH 10 for all sensors. In the reverse pH from basic to acidic region, the OCP is similar in the surface-modified sensors

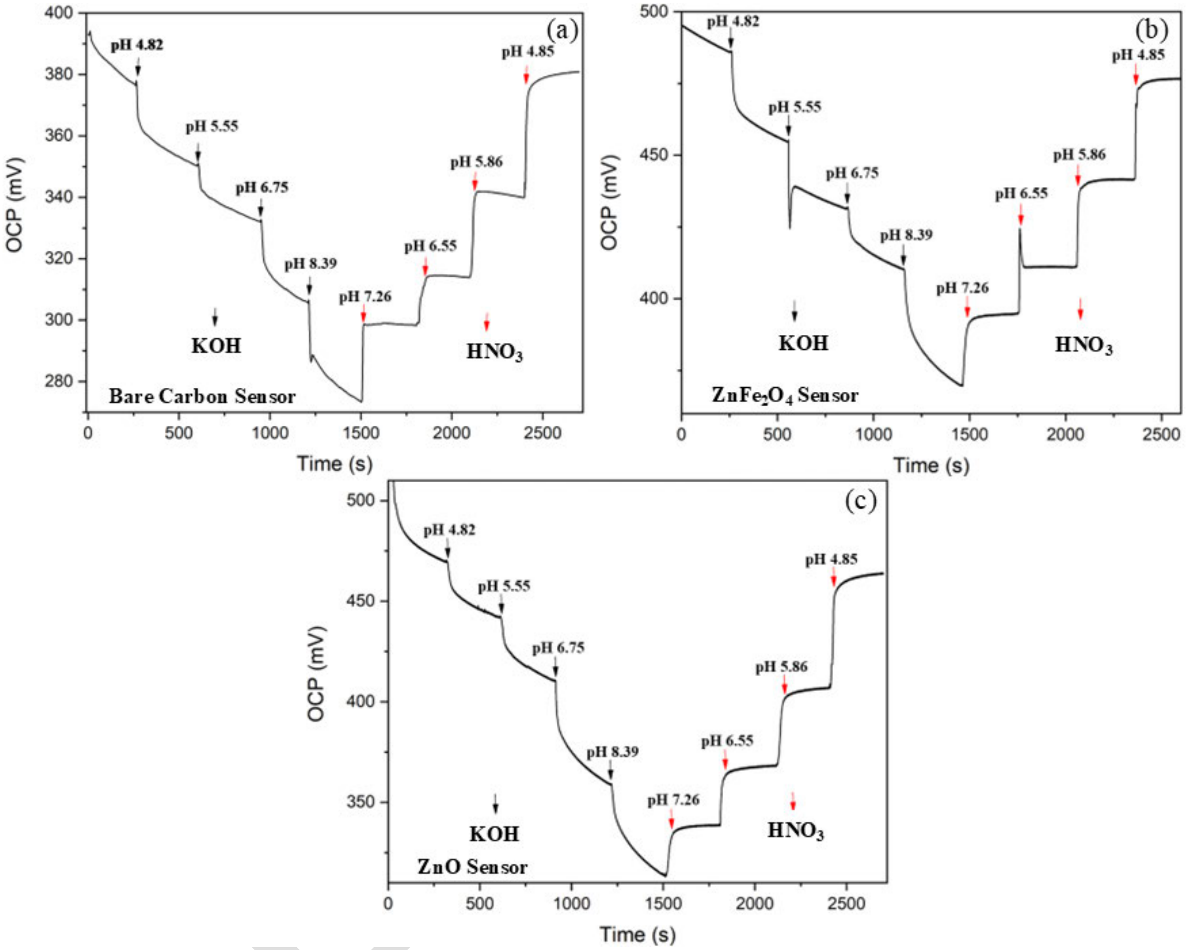

Fig. 7. Chronopotentiometric response of (a) bare, (b) $ZnFe_2O_4$, and (c) ZnO pH sensors with reduced hysteresis effect in pH loop 4.5–8.5–4.5.

compared to the initial OCP from acidic to basic region. These differences in response leads to a phenomenon called "hysteresis" in pH sensors especially in the case of metal oxide-based pH sensors [6]. The potential difference from initial response to the final response in the complete pH loop is called the "hysteresis width" as indicated in Fig. 6. The ZnO-based sensor has the highest hysteresis width of 133 mV, bare carbon sensor has the lowest width of 39 mV, and the $ZnFe_2O_4$-based sensor has a hysteresis width of 81 mV. The hysteresis width defines the functionality of a pH sensor and the pH range in which the sensor can be utilized. The lower the hysteresis width, the better the performance of the sensor in that pH range. As reported before, the hysteresis behavior depends on the pH looping (pH range in which the sensor is operated) [38]. Since our main interest is in the physiological pH range, the sensors are characterized in the pH loop 4.5–8.5–4.5 (with nine different pH values with a total time span of 45 min) as shown in Fig. 7. It is clearly observed that the hysteresis behavior is reduced to 3, 18, and 44 mV for bare carbon, $ZnFe_2O_4$, and ZnO-based sensors, respectively. This is significantly lower compared to the previous pH loop proving that the hysteresis behavior is pH loop-dependent.

Stability of the pH sensors is another important performance factor. As is clear from Figs. 6 and 7, the potentiometric response is not reaching a steady-state value when the pH is changing from lower to higher values by the addition of KOH solution. To understand the sensors' stability, the response is recorded at different pH values for longer times (10 and 20 min after each change in pH value) as presented in Fig. 8. A drift over time is still observed without reaching any steady-state value. The response starts to stabilize immediately after the addition of HNO_3 solution into the solution under test. To understand this effect, it is important to consider how a pH sensor works. When the sensor is immersed into the test solution, the hydroxide (OH^-) ions get attracted by the electrode surface due to the dissociative adsorption of water. This adsorption leads to a potential difference between the WE and the RE. Due to the addition of more KOH solution into the test UBS solution, the sensor's surface is enriched with more OH^- ions, leading to a difference in the potential between WE and RE. When the HNO_3 solution is added, the response starts to stabilize immediately as we introduce H^+ ions. This is due to the faster diffusion of H^+ ions (and so faster protonation of the electrode surface) compared to the process of interaction of OH^- ions with the electrode surface [6]. To improve the stability of the sensors, instead of using KOH as the base stock solution, bicarbonates such as $KHCO_3$ or $NaHCO_3$ can be employed. This might improve the stability of the potential response as well as the pH sensitivity of the sensors. When the pH of the solution under investigation is controlled with KOH and HNO_3, the sensors are calibrated in the pH range mentioned above to compare the OCP. When

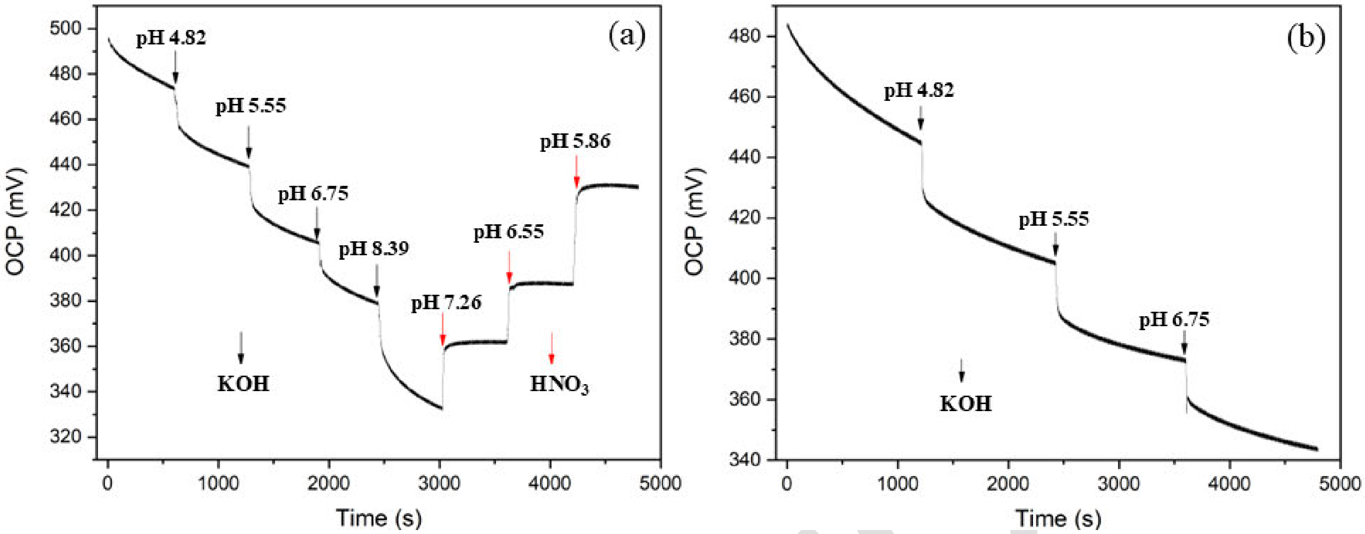

Fig. 8. Stability tests: chronopotentiometric response of $ZnFe_2O_4$ pH sensor with longer stabilization times [(a) 10 and (b) 20 minutes of waiting time in between subsequent pH changes] after each pH change in the range between 4.5 and 8.5.

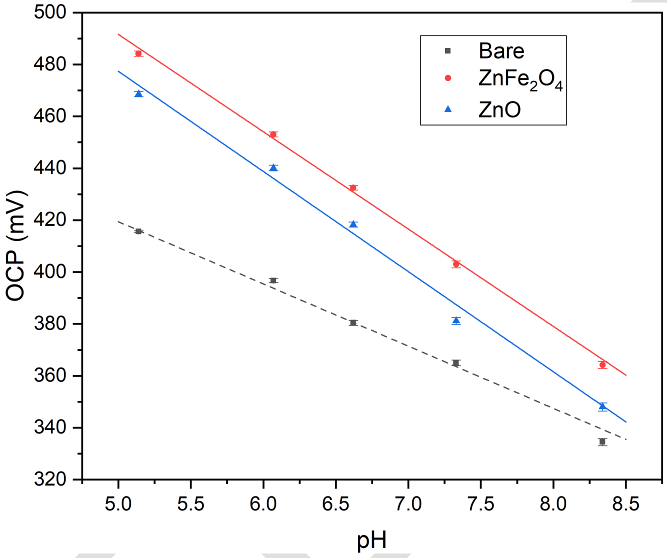

Fig. 9. Calibration of bare carbon, $ZnFe_2O_4$, and ZnO pH sensors in the pH between 5 and 8.5.

HNO_3 is used after KOH in continuous measurements, the sensitivity of the sensors is higher, according to the calibration plots shown in Fig. S8. However, this is unreliable because the OCP response is unstable in the first case when KOH is used, which affects the OCP levels in the second case when HNO_3 is used for pH control. The response time of the sensors is difficult to investigate due to unstable response in the case of KOH; therefore, the response time is reported for the second case when HNO_3 is used for pH control. The bare, $ZnFe_2O_4$, and ZnO-based sensors showed response times (T_{95}) of 5, 80, and 95 s, respectively. These times are just indicative but not reliable due to unstable continuous OCP measurements with KOH for pH control.

To assess the performance of the electrodes as pH sensors, three freshly prepared electrodes of each type are taken, and the potential response is measured for three minutes as reported in Fig. S9. The average potential response in the last 60 s before changing the pH is considered to calibrate the sensors in the pH range between 5 and 8.5. pH calibration of the sensors is presented in Fig. 9. Bare carbon sensor, $ZnFe_2O_4$, and ZnO-based sensors have shown sensitivities of 23.9 ± 1.4, 37.3 ± 1.1, and 38.1 ± 1.3 mV/pH, respectively. The presence of either $ZnFe_2O_4$ or ZnO significantly improved the pH sensing performance of bare carbon sensor, resulting in an increase of sensitivity of around 60%. pH sensing response is usually analyzed with the Nernst equation [6] as written below

$$E = E_0 - \frac{2.303RT}{nF}\,\text{pH} \tag{1}$$

where E is the Nernst potential, E_0 is the standard surface potential, R is the universal gas constant, T is the temperature, and "n" is the number of electrons transferred in the reaction. At atmospheric conditions with $T = 25$ °C for one electron process (i.e., $n = 1$), the slope of the plot (E versus pH) is 59 mV/pH. This response is usually termed as Nernstian response for pH. Though for our sensors the response is not Nernstian, we observed a significant increase with respect to bare sensor, proving the potential of $ZnFe_2O_4$ or ZnO in pH sensing applications.

The ZnO particles have a pyramid shape where the sides and long edges of the particles are electroactive, whereas $ZnFe_2O_4$ has (close to) uniform spherical-shaped particles. Another difference is in the crystal structure which is hexagonal for ZnO microparticles, while $ZnFe_2O_4$ particles exhibit a complex normal spinel where the metal centers of Fe and Zn play an important role in the electrochemical activity of the sensors [24], [39]. ZnO is a wide bandgap material (either p- or n-type semiconductor) with a bandgap around 3.2 eV [40], whereas $ZnFe_2O_4$ (n-type semiconductor) has a smaller bandgap of about 2.5 eV [25], [26]. Even though they have these differences, we have observed that a comparable electroactive surface area (from ferri/ferrocyanide sensing), charge transfer resistance [kinetic limited reactions without diffusion limitations from Nyquist plots (see Fig. 4)], electron transfer rate constant ("k") and sensitivity in pH sensing for

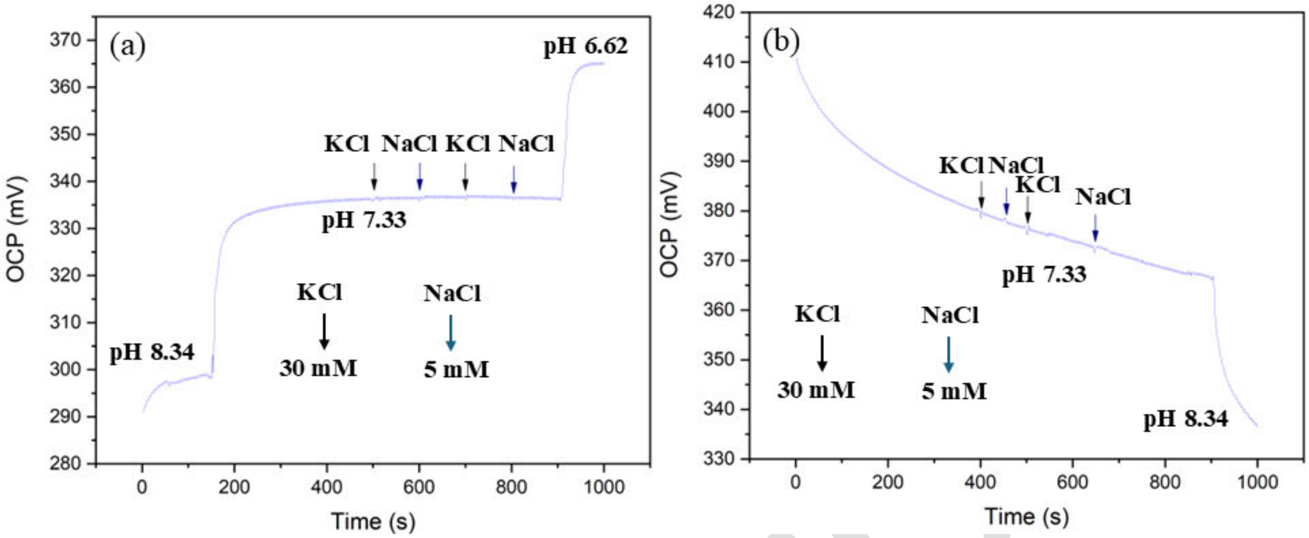

Fig. 10. Interference tests for $ZnFe_2O_4$ pH sensor by adding 30 mM KCl and 5 mM NaCl in solution at neutral pH. The tests are performed by changing the pH from (a) basic to neutral pH and (b) neutral to basic pH.

our $ZnFe_2O_4$ and ZnO -based sensors. ZnO-based sensor has shown higher hysteresis width compared to the other two types of sensors in this work. For the selection of the electrode type, it is crucial to consider eventual metal oxide dissolution effects. The dissolution depends on the metal solubility in the solution and the loading of the nanoparticle/microparticle on the surface [41]. ZnO can dissociate into Zn(II) and $Zn(OH)^+$ ions in aqueous solutions with alkaline or neutral pH conditions [40], [41], [42], [43]. On the other hand, there is no evidence of dissolution of $ZnFe_2O_4$ reported so far in the literature. Thus, interference tests are performed with the $ZnFe_2O_4$-based sensor by using relevant interferent species, namely KCl and NaCl, at the physiological pH of 7.33 (close to the blood pH of 7.4). The measurement graph is shown in Fig. 10. During the measurement, 30 mM KCL is added followed by the successive addition of 5 mM NaCl. There is no significant effect on the potential response of the sensor proving an excellent pH sensing selectivity to interfering ions. In this work, we used the simple auto-combustion synthesis method to produce ZnO and $ZnFe_2O_4$ particles based on our previous work [25], [26]. The electrochemical pH sensor response of the SPEs is improved by modification with the synthesized micromaterial/nanomaterial. The performance of the sensors can be further improved to have more control over the particle growth kinetics and the material structural properties. For instance, using appropriately selected surfactants during the synthesis can reduce particle aggregation. This would lead to an improvement in particle activity when incorporated on the electrode surface.

IV. CONCLUSION

In this work, ZnO and $ZnFe_2O_4$ particles are successfully produced using a simple and cost-effective auto-combustion synthesis method. The materials are characterized by FESEM and XRD to understand their morphological and structural features. Commercial SPEs were modified with the developed particles and studied as new electrochemical sensors. First, the sensors are characterized using ferri/ferrocyanide redox couple as a probe molecule *via* CV. Significant enhancement in the performance of bare carbon sensor is achieved in terms of sensitivity and rate constant using ZnO or $ZnFe_2O_4$ particles. Successively, the electrodes' performance as pH sensor is studied by means of chronopotentiometric measurements. The hysteresis behavior of the sensors is improved by using the physiological pH loop (4.5–8.5–4.5). We observed that the stability of the pH sensors is affected by the addition of OH^- ions in the test solution. Because of this, we propose the use of alternative stock solutions for pH change to obtain a stable steady-state signal upon the increase in the pH. Overall, the pH sensitivity of bare carbon sensor is increased (>55%) by using two different surface-modified sensors (ZnO or $ZnFe_2O_4$). Due to potential dissolution issues of the ZnO particles when in water-based solution and reduced hysteresis in pH sensing, interference studies are conducted at $ZnFe_2O_4$-modified electrodes and shown that the sensor is silent to potentially relevant interfering ions.

In this work, we choose to study $ZnFe_2O_4$ due to its chemical stability, easy processing, low-cost synthesis, high surface area at nanoscale, easily tunable structure, and its n-type semiconducting and ferromagnetic nature with normal spinel structure. For continuous monitoring, no dissolution is expected due to its highly stable closely packed face-centered cubic structure which is crucial in pH sensing. Additionally, by incorporating surfactants in the synthesis process (hydrothermal or co-precipitation or sol–gel method), agglomeration can be avoided leveraging nanoscale properties which can lead to improved performance in the future work.

ACKNOWLEDGMENT

Mallikarjun Madagalam is with the Department of Physics and Astronomy (Semiconductor Physics), KU Leuven—University of Leuven, 3001 Leuven, Belgium, also with the Department of Applied Science and Technology, Politecnico di Torino, 10129 Turin, Italy, also with the Bio/CMOS Interfaces Laboratory, École Polytechnique Fédérale de Lausanne, 2000 Lausanne, Switzerland, and also with the National Interuniversity Consortium of Materials Science and Technology—Unit of Torino, Politecnico di Torino, 50121 Florence, Italy (e-mail: mallikarjun.madagalam@polito.it).

AQ:4
AQ:5

Filippo Franceschini is with the Department of Physics and Astronomy (Semiconductor Physics), KU Leuven—University of Leuven, 3001 Leuven, Belgium.

Catarina Fernandes is with the Department of Electrical Engineering (Micro and Nano Systems), KU Leuven—University of Leuven, 3001 Leuven, Belgium.

Michele Rosito is with the Department of Applied Science and Technology, Politecnico di Torino, 10129 Turin, Italy.

Elisa Padovano is with the Department of Applied Science and Technology, Politecnico di Torino, 10129 Turin, Italy, and also with the National Interuniversity Consortium of Materials Science and Technology—Unit of Torino, Politecnico di Torino, 50121 Florence, Italy.

Sandro Carrara is with the Bio/CMOS Interfaces Laboratory, École Polytechnique Fédérale de Lausanne, 2000 Lausanne, Switzerland.

Alberto Tagliaferro is with the Department of Applied Science and Technology, Politecnico di Torino, 10129 Turin, Italy, also with the National Interuniversity Consortium of Materials Science and Technology—Unit of Torino, Politecnico di Torino, 50121 Florence, Italy, and also with the Faculty of Science, Ontario Tech University (OntarioTechU), Oshawa, ON L1G 0C5, Canada.

Mattia Bartoli is with the National Interuniversity Consortium of Materials Science and Technology—Unit of Torino, Politecnico di Torino, 50121 Florence, Italy, and also with the Center for Sustainable Future Technologies, Italian Institute of Technology, 10144 Turin, Italy.

Irene Taurino is with the Department of Physics and Astronomy (Semiconductor Physics) and the Department of Electrical Engineering (Micro and Nano Systems), KU Leuven—University of Leuven, 3001 Leuven, Belgium.

REFERENCES

[1] M. T. Ghoneim et al., "Recent progress in electrochemical pH-sensing materials and configurations for biomedical applications," *Chem. Rev.*, vol. 119, no. 8, pp. 5248–5297, Mar. 2019, doi: 10.1021/acs.chemrev.8b00655.

[2] D. Wencel, T. Abel, and C. McDonagh, "Optical chemical pH sensors," *Anal. Chem.*, vol. 86, no. 1, pp. 15–29, Jan. 2014, doi: 10.1021/ac4035168.

[3] Y. Qin, H.-J. Kwon, M. M. R. Howlader, and M. J. Deen, "Microfabricated electrochemical pH and free chlorine sensors for water quality monitoring: Recent advances and research challenges," *RSC Adv.*, vol. 5, no. 85, pp. 69086–69109, 2015, doi: 10.1039/c5ra11291e.

[4] Y. Qin et al., "Integrated water quality monitoring system with pH, free chlorine, and temperature sensors," *Sens. Actuators B, Chem.*, vol. 255, pp. 781–790, Feb. 2018, doi: 10.1016/j.snb.2017.07.188.

[5] M. Weston, S. Geng, and R. Chandrawati, "Food sensors: Challenges and opportunities," *Adv. Mater. Technol.*, vol. 6, no. 5, May 2021, Art. no. 2001242, doi: 10.1002/admt.202001242.

[6] L. Manjakkal, D. Szwagierczak, and R. Dahiya, "Metal oxides based electrochemical pH sensors: Current progress and future perspectives," *Prog. Mater. Sci.*, vol. 109, Apr. 2020, Art. no. 100635, doi: 10.1016/j.pmatsci.2019.100635.

[7] M. Yuqing, C. Jianrong, and F. Keming, "New technology for the detection of pH," *J. Biochem. Biophys. Methods*, vol. 63, no. 1, pp. 1–9, Apr. 2005, doi: 10.1016/j.jbbm.2005.02.001.

[8] P. Kurzweil, "Metal oxides and ion-exchanging surfaces as pH sensors in liquids: State-of-the-art and outlook," *Sensors*, vol. 9, no. 6, pp. 4955–4985, Jun. 2009, doi: 10.3390/s90604955.

[9] S. Zaman, M. H. Asif, A. Zainelabdin, G. Amin, O. Nur, and M. Willander, "CuO nanoflowers as an electrochemical pH sensor and the effect of pH on the growth," *J. Electroanal. Chem.*, vol. 662, no. 2, pp. 421–425, Nov. 2011, doi: 10.1016/j.jelechem.2011.09.015.

[10] L. Manjakkal, K. Cvejin, J. Kulawik, K. Zaraska, D. Szwagierczak, and R. P. Socha, "Fabrication of thick film sensitive RuO_2-TiO_2 and Ag/AgCl/KCl reference electrodes and their application for pH measurements," *Sens. Actuators B, Chem.*, vol. 204, pp. 57–67, Dec. 2014, doi: 10.1016/j.snb.2014.07.067.

[11] J. Bai and B. Zhou, "Titanium dioxide nanomaterials for sensor applications," *Chem. Rev.*, vol. 114, no. 19, pp. 10131–10176, Oct. 2014, doi: 10.1021/cr400625j.

[12] A. Wei, L. Pan, and W. Huang, "Recent progress in the ZnO nanostructure-based sensors," *Mater. Sci. Eng., B*, vol. 176, no. 18, pp. 1409–1421, Nov. 2011, doi: 10.1016/j.mseb.2011.09.005.

[13] I. Yaroshenko et al., "Real-time water quality monitoring with chemical sensors," *Sensors*, vol. 20, no. 12, p. 3432, Jun. 2020, doi: 10.3390/s20123432.

[14] S. Al-Hilli and M. Willander, "The pH response and sensing mechanism of n-type ZnO/electrolyte interfaces," *Sensors*, vol. 9, no. 9, pp. 7445–7480, Sep. 2009, doi: 10.3390/s90907445.

[15] J. Chou et al., "Characterization of flexible arrayed pH sensor based on nickel oxide films," *IEEE Sensors J.*, vol. 18, no. 2, pp. 605–612, Jan. 2018, doi: 10.1109/JSEN.2017.2773143.

[16] L. Manjakkal, B. Sakthivel, N. Gopalakrishnan, and R. Dahiya, "Printed flexible electrochemical pH sensors based on CuO nanorods," *Sens. Actuators B, Chem.*, vol. 263, pp. 50–58, Jun. 2018, doi: 10.1016/j.snb.2018.02.092.

[17] H.-J. Chung et al., "Stretchable, multiplexed pH sensors with demonstrations on rabbit and human hearts undergoing ischemia," *Adv. Healthcare Mater.*, vol. 3, no. 1, pp. 59–68, Jan. 2014, doi: 10.1002/adhm.201300124.

[18] L. Manjakkal, K. Cvejin, J. Kulawik, K. Zaraska, D. Szwagierczak, and G. Stojanovic, "Sensing mechanism of RuO_2–SnO_2 thick film pH sensors studied by potentiometric method and electrochemical impedance spectroscopy," *J. Electroanal. Chem.*, vol. 759, pp. 82–90, Dec. 2015, doi: 10.1016/j.jelechem.2015.10.036.

[19] L. Manjakkal, E. Djurdjic, K. Cvejin, J. Kulawik, K. Zaraska, and D. Szwagierczak, "Electrochemical impedance spectroscopic analysis of RuO_2 based thick film pH sensors," *Electrochimica Acta*, vol. 168, pp. 246–255, Jun. 2015, doi: 10.1016/j.electacta.2015.04.048.

[20] C.-W. Pan, J.-C. Chou, T.-P. Sun, and S.-K. Hsiung, "Development of the real-time pH sensing system for array sensors," *Sens. Actuators B, Chem.*, vol. 108, nos. 1–2, pp. 870–876, Jul. 2005, doi: 10.1016/j.snb.2004.11.087.

[21] L. Santos et al., "WO_3 nanoparticle-based conformable pH sensor," *ACS Appl. Mater. Interface*, vol. 6, no. 15, pp. 12226–12234, Aug. 2014, doi: 10.1021/am501724h.

[22] C. Fernandes et al., "Unraveling the potential of a nanostructured Tungsten–Tungsten oxide thin film electrode as a bioresorbable multichemical wound healing monitor," *Adv. Mater. Technol.*, vol. 9, no. 10, May 2024, Art. no. 2302007, doi: 10.1002/admt.202302007.

[23] J. Kim et al., "Structural insights into multi-metal spinel oxide nanoparticles for boosting oxygen reduction electrocatalysis," *Adv. Mater.*, vol. 34, no. 8, Feb. 2022, Art. no. 2107868, doi: 10.1002/adma.202107868.

[24] J. M. Gonçalves et al., "Sensing performances of spinel ferrites MFe_2O_4 (M = Mg, Ni, Co, Mn, Cu and Zn) based electrochemical sensors: A review," *Analytica Chim. Acta*, vol. 1233, Nov. 2022, Art. no. 340362, doi: 10.1016/j.aca.2022.340362.

[25] M. Madagalam et al., "Unraveling the effect of the chemical and structural composition of $Zn_xNi_{1-x}Fe_2O_4$ on the electron transfer at the electrochemical interface," *Small Struct.*, vol. 4, no. 12, Dec. 2023, Art. no. 2300163, doi: 10.1002/sstr.202300163.

[26] M. Madagalam et al., "Unveiling the effect of bi in $ZnFe_2O_4$ nanoparticles in electrochemical sensors," *Appl. Surf. Sci.*, vol. 673, Nov. 2024, Art. no. 160870, doi: 10.1016/j.apsusc.2024.160870.

[27] M. Madagalam et al., "Enhancing electrochemical sensor performance: Studies of electrodes tailored with ZnO/$ZnFe_2O_4$ nanoparticles," *Meet. Abstr.*, vol. 245, no. 47, p. 2627, Aug. 2024, doi: 10.1149/MA2024-01472627mtgabs.

[28] M. Kumar, B. E. Kumara Swamy, C. Sravanthi, C. M. Praveen Kumar, and G. K. Jayaprakash, "$NiFe_2O_4$ nanoparticle modified electrochemical sensor for the voltammetric study of folic acid and paracetamol," *Mater. Chem. Phys.*, vol. 284, May 2022, Art. no. 126087, doi: 10.1016/j.matchemphys.2022.126087.

[29] N. T. Anh et al., "An on-site and portable electrochemical sensing platform based on spinel zinc ferrite nanoparticles for the quality control of paracetamol in pharmaceutical samples," *Nanosc. Adv.*, vol. 6, no. 1, pp. 256–267, 2024, doi: 10.1039/d3na00749a.

[30] M. Amiri, M. Salavati-Niasari, and A. Akbari, "Magnetic nanocarriers: Evolution of spinel ferrites for medical applications," *Adv. Colloid Interface Sci.*, vol. 265, pp. 29–44, Mar. 2019, doi: 10.1016/j.cis.2019.01.003.

[31] M. Madagalam, M. Bartoli, S. Carrara, and A. Tagliaferro, "$ZnCr_{2-x}Fe_xO_4$ nanoparticles-modified electrochemical sensors: A comparative study," in *Proc. IEEE Sensors*, Oct. 2023, pp. 1–4, doi: 10.1109/sensors56945.2023.10325135.

[32] M. Madagalam, M. Bartoli, S. Carrara, and A. Tagliaferro, "$ZnM_xFe_{2-x}O_4$ (M=Cr, Bi) nanoparticles-modified electrochemical sensors: Effect on sensitivity and first-order kinetic rate constant," in *Proc. IEEE BioSensors Conf. (BioSensors)*, Jul. 2023, pp. 1–4, doi: 10.1109/biosensors58001.2023.10280910.

[33] A. C. F. M. Costa, E. Tortella, M. R. Morelli, M. Kaufman, and R. H. G. A. Kiminami, "Effect of heating conditions during combustion synthesis on the characteristics of $Ni_{0.5}Zn_{0.5}Fe_2O_4$ nanopowders," *J. Mater. Sci.*, vol. 37, no. 17, pp. 3569–3572, Sep. 2002, doi: 10.1023/a:1016528302082.

[34] A. J. Bard and L. R. Faulkner, *Electrochemical Methods Fundamentals and Applications*. Newyork, NY, USA: Wiley, 2001.

[35] R. S. Nicholson, "Theory and application of cyclic voltammetry for measurement of electrode reaction kinetics," *Anal. Chem.*, vol. 37, no. 11, pp. 1351–1355, Oct. 1965.

[36] M. Madagalam, M. Bartoli, A. Tagliaferro, and S. Carrara, "Bismuth-nanocomposites modified SPCEs for non-enzymatic electrochemical sensors," *IEEE Sensors J.*, vol. 21, no. 9, pp. 11155–11162, May 2021, doi: 10.1109/JSEN.2021.3059278.

[37] E. Laviron, "General expression of the linear potential sweep voltammogram in the case of diffusionless electrochemical systems," *J. Electroanal. Chem. Interfacial Electrochemistry*, vol. 101, no. 1, pp. 19–28, Jul. 1979, doi: 10.1016/s0022-0728(79)80075-3.

[38] C.-N. Tsai, J. C. Chou, T. P. Sun, and S. K. Hsiung, "Study on the time-dependent slow response of the tin oxide pH electrode," *IEEE Sensors J.*, vol. 6, no. 5, pp. 1243–1249, Oct. 2006, doi: 10.1109/JSEN.2006.881364.

[39] C. Fan et al., "Synthesis and electrocatalytic mechanism of ultrafine MFe_2O_4 (M: Co, Ni, and Zn) nanocrystallites: M/Fe synergistic effects on the electrochemical detection of Cu(ii) and hydrogen evolution reaction performances," *J. Mater. Chem. A*, vol. 9, no. 39, pp. 22277–22290, 2021, doi: 10.1039/d1ta05646h.

[40] H. Zhang et al., "Use of metal oxide nanoparticle band gap to develop a predictive paradigm for oxidative stress and acute pulmonary inflammation," *ACS Nano*, vol. 6, no. 5, pp. 4349–4368, May 2012, doi: 10.1021/nn3010087.

[41] M. Auffan, J. Rose, M. R. Wiesner, and J.-Y. Bottero, "Chemical stability of metallic nanoparticles: A parameter controlling their potential cellular toxicity in vitro," *Environ. Pollut.*, vol. 157, no. 4, pp. 1127–1133, Apr. 2009, doi: 10.1016/j.envpol.2008.10.002.

[42] T. Xia et al., "Decreased dissolution of ZnO by iron doping yields nanoparticles with reduced toxicity in the rodent lung and zebrafish embryos," *ACS Nano*, vol. 5, no. 2, pp. 1223–1235, Feb. 2011, doi: 10.1021/nn1028482.

[43] T. Xia et al., "Comparison of the mechanism of toxicity of zinc oxide and cerium oxide nanoparticles based on dissolution and oxidative stress properties," *ACS Nano*, vol. 2, no. 10, pp. 2121–2134, Oct. 2008, doi: 10.1021/nn800511k.

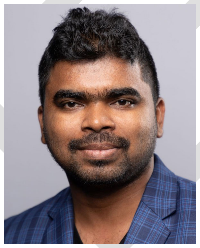

AQ:6

Mallikarjun Madagalam (Student Member, IEEE) received the bachelor's degree in electronics and communication engineering from the Rajiv Gandhi University of Knowledge Technologies, Nuzvid, India, in 2014, the first master's degree in electronics from Halmstad University, Halmstad, Sweden, in 2017, and the second master's degree in nanotechnologies for ICTs from Politecnico di Torino, Turin, Italy, and from 2020, he pursued the Ph.D. degree on the effect of spinel nanomaterials on electron transfer at the electrochemical interfaces.

From November 2016 to February 2017, he was a Research Engineer with Halmstad University. While pursuing his second master's degree in Italy, he received full scholarship, international mobility grant from EDISU, and thesis abroad scholarship from Politecnico di Torino. From 2020 to 2021, he was a Research Assistant with the Sensing Technologies Laboratory of Prof. Paolo Lugli, Free University of Bolzano, Bolzano, Italy. During his Ph.D., he spent a period in the electrochemistry group of Prof. Irene Taurino at KU Leuven, Leuven, Belgium, and another period in the Bio/CMOS Interfaces Laboratory of Prof. Sandro Carrara at École Polytechnique Fédérale de Lausanne (EPFL), Lausanne, Switzerland.

Mr. Madagalam was awarded the Global Swede Award in 2016 by Swedish Ministry of Foreign Affairs and the Swedish Institute.

Filippo Franceschini (Student Member, IEEE) received the B.Sc. degree in mechanical engineering from the Università degli Studi di Brescia, Brescia, Italy, and the M.Sc. (summa cum laude) degree in materials engineering from the Polytechnic University of Turin, Turin, Italy. He is currently pursuing the Ph.D. degree in physics with KU Leuven, Leuven, Belgium, as an FWO Fellow (Strategic Basic Research).

AQ:7 AQ:8

His research focuses on the intersection of materials science and electrocatalysis, with a particular emphasis on nonenzymatic electrooxidation of organic molecules.

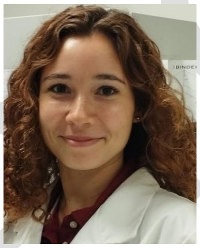

Catarina Fernandes received the B.Sc. degree in micro- and nanotechnology engineering from the NOVA School of Science and Technology, NOVA University Lisbon, Portugal, in 2019, and the M.Sc. degree in nanoscience from Aarhus University, Aarhus, Denmark, in 2021. She is currently the Ph.D. degree with the Micro and Nano-Systems (MNS) Research Group, KU Leuven, Leuven, Belgium, under the supervision of Prof. Irene Taurino.

Her research focuses on developing novel materials and microfabrication techniques for implantable, bioresorbable electrochemical sensors.

Michele Rosito received the B.Sc. and M.Sc. degrees in materials engineering from Politecnico di Torino, Turin, Italy, in 2013 and 2020, respectively, where he is currently pursuing the Ph.D. degree in materials science and technology with the Department of Applied Science and Technology.

His current research interests include metal additive manufacturing, with a focus on laser powder bed fusion, aluminum alloys, and metal matrix composites, as well as materials characterization through XRD analysis.

Elisa Padovano received the master's degree in environmental and cultural heritage chemistry from the University of Turin, Turin, Italy, in 2010, and the Ph.D. degree in materials science and technology from the Polytechnic University of Turin, Turin, in 2015.

In January 2011, she started her research fellowship at Polytechnic University of Turin. She is an Associate Professor at Politecnico di Torino, Turin. She is the author or co-author of more than 40 scientific articles published in international peer-review journals, and various presentations in international and national conferences in the field of materials science and engineering. Her research activity mainly focused on the investigation of the processing–structure–properties relationship of advanced materials fabricated by additive manufacturing techniques. She gained experience in the processing and characterization of innovative materials for different applications. The research activity is mainly focused on 1) the development of new polymer-based composites to be processed by selective laser sintering and fused filament fabrication techniques and 2) the processing of innovative metal materials by powder bed fusion technologies.

Sandro Carrara (Fellow, IEEE) received the AQ:9 Ph.D. degree in biochemistry and biophysics from the University of Padua, Padua, Italy, the master's degree in physics from the University of Genoa, Genoa, Italy, and the diploma degree in electronics from the National Institute of Technology, Albenga, Italy.

He was a former Professor with the University of Genoa and the University of Bologna, Bologna, Italy. From 2013 to 2014, he was appointed as a CASS Distinguished Lecturer and from 2017 to 2019, he was a IEEE Sensors Council Distinguished Lecturer. He is a Professor with the École Polytechnique Fédérale de Lausanne (EPFL), Lausanne, Switzerland, where he is the Head of the Bio/CMOS Interfaces Laboratory. His work has constantly received international recognition with several best-cited papers and best conference papers. Throughout his career, he published seven books with prestigious publishers such as Springer/NATURE and Cambridge University Press. He has more than 400 scientific publications and is the author of 19 patents/patent-requests.

Dr. Carrara is a member of the IEEE Sensors Council, where he was the Vice President of Publications. He also was a member of the Board of Governors (BoG) of the IEEE Circuits and Systems Society (CASS). He is the recipient of the IEEE Sensors Council Technical Achievement Award in 2016, and the Scientist Medal by the International Association of Advanced Materials in 2024. He has been the General Chairman of AQ:10 the premier worldwide international conference in the area of circuits and systems for biomedical applications, IEEE Biomedical Circuits and Systems (BioCAS), in 2014. He also has been the General Chairman of the 16th Edition of IEEE International Symposium on Medical Measurements and Applications (MeMeA), IEEE MeMeA, in 2021. He is a former Editor-in-Chief of the IEEE SENSORS Journal, one of the largest journals among 220 IEEE publications, and an Associate Editor of IEEE TRANSACTIONS ON BIOMEDICAL CIRCUITS AND SYSTEMS. He is also former Founding Editor-in-Chief of the Springer/NATURE journal titled *NanoBioScience*.

AQ:11 **Alberto Tagliaferro** received the M.Sc. degree AQ:12 in nuclear engineering and the Ph.D. degree in physics from the Polytechnic University of Turin, Turin, Italy.

He is an Associate Professor with the Applied Science and Technology Department, Polytechnic University of Turin. He is also the Head of the Carbon Group, a research group founded in 2002 focused on production, characterization, and the application of carbon-based materials. He has published more than 200 articles on international peer-reviewed journals and has a five-year h-index of 35 as per google scholar.

Dr. Tagliaferro is a member of the Editorial Board of a number of journals. He is Chair of the Education Committee of the International Union for Vacuum Science, Technique, and Applications (IUVSTA).

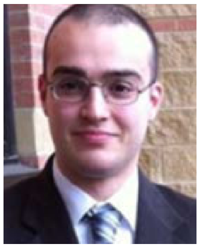

Mattia Bartoli received the M.Sc. (summa cum laude) degree in organic chemistry from the University of Florence, Florence, Italy, in 2013, and a prize for the outstanding graduation project from Italian Chemical Society, and the Ph.D. degree in chemistry from the University of Florence, in 2017.

Dr. Bartoli joined the Biorefinery Research Group, University of Alberta, where he con- AQ:13 tributed to developing new materials for catalytic applications and new technologies. During this period, he also worked as the Head of Research and Development for ForgeHydrocarbon a spin-off company of University of Alberta solving several issues of the innovative lipid-to hydrocarbon technology for renewable hydrocarbon production. Thanks to his contribution, ForgeHydrocarbon was able to move from pilot to commercial stage. In 2018, he joined the Carbon Group, Polytechnic University of Turin, Turin, Italy, where he studied both production and use of carbon from thermochemical conversion of wastestreams for material science applications. Since 2021, he has been working on nanomaterials development at the Center for Sustainable Future Technologies—CSFT@POLITO. He recognizes the interdisciplinary nature of the carbon materials research sector and puts all his efforts into developing not merely one-case solutions but platforms that could originate solution trees useful for solving complex scenarios by integrating material science. He works in collaboration with the University of Miami leading the foundation of chemical formation route of the main families of carbon dots. Since 2019, he has been in collaboration with both École Polytechnique Fédérale de Lausanne (EPFL), Lausanne, Switzerland, and Politecnico di Torino, Turin, empirical proved Markus Tachiya theory highlighting the role of surface state on electron transfer rate. He is enlisted in the World's Top 2% Scientists list.

Dr. Bartoli is a Fellow of several scientific societies.

Irene Taurino (Member, IEEE) received the B.Sc. degree in biomed- AQ:14 ical engineering from Politecnico di Torino, Turin, Italy, the dual M.Sc. (summa cum laude) degree in biomedical engineering from Politecnico di Milano, Milan, Italy, and the Ph.D. degree in microsystems and microelectronics at École Polytechnique Fédérale de Lausanne (EPFL), Lausanne, Switzerland, in 2015, under the supervision of Prof. Giovanni De Micheli and Prof. Sandro Carrara, specializing in nanotechnology, microfabrication, electrochemistry, and microfluidics.

In 2014, she was a Visiting Student at Harvard-MIT Health Sciences and Technology, Cambridge, MA, USA, integrating an electrochemical device into a microfluidic cell culture system. She later conducted postdoctoral research at EPFL, contributing to teaching and supervision. From 2016 to 2021, she was with Industrial Research and Development, Aerosol Science and Technology, filing tens of patent applications (43 AQ:15 simple families). In June 2021, she became an Assistant Professor at KU Leuven, Leuven, Italy, jointly affiliated with the Electrical Engineering and Physics and Astronomy Departments. Her research focuses on advanced micro- and nanotechnologies for soft electrochemical platforms. Since May 2023, she has also been a collaborator (10%) at the Italian Institute of Technology (IIT).